

# Quadratic Sums-of-Powers for Fixed-Parameter Tractable Quantum-Circuit Simulation\*

Alexis de Colnet<sup>1</sup>, Floris Geerts<sup>2</sup>, Rihan Hai<sup>3</sup>, Alfons Laarman<sup>1</sup>,  
Joon Hyung Lee<sup>1</sup>, and Guillermo A. Pérez<sup>†2</sup>

<sup>1</sup>Leiden University, Netherlands

<sup>2</sup>University of Antwerp, Belgium

<sup>3</sup>TU Delft, Netherlands

## Abstract

Strongly simulating a quantum circuit, that is, computing an output amplitude, amounts to summing the circuit’s Feynman paths, a weighted count over assignments to the Boolean “path” variables. The circuit’s gates induce correlations among these variables, forming a graph whose structure determines the hardness of the simulation task. This *sum-of-powers* viewpoint underlies recent simulators built on knowledge-representation tools from artificial intelligence, namely binary decision diagrams and weighted model counting. We show that the structural quantity most accurately governing the difficulty is the *rank-width* of the path-variable graph, and we give an algorithm that evaluates the amplitude in time that is exponential only in this rank-width and polynomial in the circuit size. Rank-width can be far smaller than the widths that control competing methods: as corollaries, our algorithm reproduces a recent decision-diagram simulation breakthrough as a special case and matches the Markov–Shi tensor-network contraction bound. To complement this, we exhibit circuit families on which our algorithm provably beats both competing methods. The new method applies to every circuit built from Hadamard and diagonal gates, in particular to circuits over Clifford+T. In practical terms, general-purpose decision-diagram and model-counting tools can serve as the workhorse, with our specialized algorithm dispatched to exploit a small rank-width of the associated graph when it is present.

## 1 Introduction

Classical strong simulation of quantum circuits remains indispensable: it forms a basis for circuit compilation and optimization pipelines, aids the study of noise in actual hardware, and helps triangulate truly quantum-hard regimes that are infeasible for classical machines. The difficulty lies in the fact that an  $n$ -qubit

---

\*This work was supported by the FWO/NWO KR2iQS project (G076326N), a collaboration between the University of Antwerp and Leiden University.

<sup>†</sup>Contact: [guillermo.perez@uantwerpen.be](mailto:guillermo.perez@uantwerpen.be)

state is described by  $2^n$  amplitudes; therefore, a useful simulator must exploit structure rather than represent the state naively.

Tensor-network contraction gives a standard route to strong simulation of quantum circuits. If  $N_C$  is the tensor-network graph of a circuit  $C$ , with tensor vertices and shared indices as edges, then a contraction order is naturally governed by the treewidth of the line graph  $L(N_C)$  of  $N_C$ . We write

$$\text{cc}(N_C) = \text{tw}(L(N_C))$$

for this contraction complexity. The Markov–Shi simulation bound is single-exponential in the corresponding tensor-network width parameter [MS08] and linear in the circuit size.

The route we develop instead is the *sum-of-powers* (SOP): the expression of an amplitude as a sum over Feynman paths. This representation is classical [DHM<sup>+</sup>05], but it has recently been turned into competitive simulators by encoding it with knowledge-representation tools from artificial intelligence: e.g. binary decision diagrams, in FeynmanDD [WCYJ25, CWD<sup>+</sup>25], and weighted model counting [vdELLB26, MBL24, QMCL24, HCC<sup>+</sup>26]. Fixing the circuit’s input  $\mathbf{y}$  and output  $\mathbf{z}$  turns the circuit into a scalar

$$Z = \frac{1}{R} \sum_{\mathbf{x} \in \{0,1\}^V} \omega_r^{f(\mathbf{x})},$$

a sum of roots of unity over assignments to a set  $V$  of Boolean path variables; the exponent  $f$  is a degree-two polynomial: a constant, one linear term per variable, and a quadratic sign term for each interacting pair of variables (for  $\{H, T, CZ\}$  the modulus is  $r = 8$ , see Section 3). The interacting pairs form the *SOP variable graph*  $G_C = (V, E)$ , and the difficulty of evaluating  $Z$  is concentrated in the structure of this graph.

Our main result is that the right structural measure of  $G_C$  is its *rank-width*, a branching width parameter from structural graph theory. We give a dynamic program (Section 4) that evaluates  $Z$ , hence the amplitude, in time exponential only in the rank-width of  $G_C$  and polynomial in the circuit size.

**Contributions.** We establish the following based on parameters in Table 1:

1. We give an explicit rank-decomposition dynamic program for quadratic SOPs, running in time  $O(nr4^k \text{poly}(n) + r \log r)$  on an  $n$ -variable graph of rank-width  $k$  and modulus  $r$  (Theorem 2, Theorem 3), when provided with a rank-width decomposition. Applied to circuits over Hadamard and diagonal gates, this is a rank-width fixed-parameter strong simulation algorithm (Section 6). On the way, we also expose a treewidth fixed-parameter strong simulation algorithm by combining the insight that  $G_C$  is the “primal graph” of the SOP with classical graphical-model algorithms (Section 3.2).
2. We relate the SOP variable graph to the parameters of the tensor-network and decision-diagram approaches:  $G_C$  is a minor of the tensor line graph, giving  $\text{tw}(G_C) \leq \text{cc}(N_C)$  (Lemma 1) and  $\text{rw}(G_C) \leq \text{cc}(N_C) + 1$  [Oum08]; and since rank-width is at most linear rank-width, we recover the decision-diagram guarantee of [CWD<sup>+</sup>25] (Corollary 1) as a special case.

3. We construct circuit families with  $\text{rw}(G_C) = O(1)$  while  $\text{lrw}(G_C)$  and  $\text{cc}(N_C)$  are unbounded (Corollary 2), explicitly separating the rank-width, linear-rank-width, and treewidth approaches. On these families, our rankwidth-parameterized algorithm runs with fixed polynomial overhead, whereas decision-diagram and tensor-network guarantees both degrade.

Although we state the construction for the  $\{\text{H}, \text{T}, \text{CZ}\}$  gate set, it requires only that the Hadamard gate is the sole non-diagonal single-qubit gate. In fact, arbitrary diagonal single-qubit gates contribute linear terms but leave  $G_C$  unchanged. The results therefore cover every circuit over Hadamard, CZ, and arbitrary phase rotation gates, and in particular all of Clifford+T (Section 6.2).

**Other related work.** Weighted model counting has recently been proposed as a general framework for quantum physics computations, including partition functions [vdELLB26]; the present work uses such encodings as one practical route and contributes a rank-width fixed-parameter algorithm for the underlying SOP. Recent and independent work has also identified rank-width as a useful parameter for quantum-circuit simulation, mainly through ZX-calculus and stabilizer-decomposition methods. Kuyanov and Kissinger [KK26] give a contraction algorithm for graph-like ZX diagrams whose claimed running time is  $\tilde{O}(4^R)$  given a rank-decomposition of width  $R$ . Codsì and Laakkonen [CL26] develop a framework connecting graph-width measures and stabilizer decompositions, obtaining slice-wise polynomial-time algorithms parameterized by treewidth or rank-width of an associated tensor network together with the number of non-Clifford operations. These results are complementary to ours: they show, from a ZX/tensor-network perspective, that rank-width is a natural structural parameter for simulation. Our contribution is different in that we work directly with the quadratic SOP representation underlying FeynmanDD-style simulation; give an explicit DP that runs on a rank-decomposition of the SOP variable graph  $G_C$ ; and relate this graph to both graphical-model treewidth and tensor-network contraction complexity. In particular, T and other single-qubit diagonal gates enter the SOP only as unary phases and leave  $G_C$  unchanged, so the number of non-Clifford gates affects our running time only polynomially, through the circuit size, and never in the exponent.

Table 1: Graph objects used in the paper. Treewidth travels from tensor network to the SOP variable graph via  $L(N_C)$ ; rank-width is used directly on  $G_C$ .

Graph	Definition	Relation used here
$N_C$	Tensor-network graph: tensors are vertices and shared indices are edges.	Tensor contraction is measured through the line graph. For bounded tensor arity $\Delta$ , $\text{tw}(L(N_C)) \leq \Delta(\text{tw}(N_C) + 1) - 1$ .
$L(N_C)$	Line graph of $N_C$ : vertices are the bond indices (edges of $N_C$ ); adjacency means co-occurrence in a tensor.	$\text{cc}(N_C) = \text{tw}(L(N_C))$ . The SOP variable graph $G_C$ is a minor of $L(N_C)$ .
$G_C$	SOP variable graph: vertices are the SOP variables $V$ ; edges are the quadratic cross-terms $\{u, v\} \in E$ in $f$ .	The rank-width dynamic-programming algorithm (DP) runs on this graph. Also $\text{tw}(G_C) \leq \text{cc}(N_C)$ .

## 2 Preliminaries

This section collects the two ingredients the rest of the paper relies on: the graph width parameters that will measure simulation cost and the quantum circuits we simulate together with their tensor-network representation. A reader already comfortable with these notions can skim and refer back as needed.

### 2.1 Graph notation and parameters

We first collect the graph notation and width parameters used throughout the paper. All graphs are finite, undirected, and simple unless explicitly stated otherwise. For a graph  $G = (V, E)$  and sets  $S, T \subseteq V$ ,  $\mathbf{A}_G[S, T]$  denotes the submatrix of the adjacency matrix of  $G$  with rows indexed by  $S$  and columns indexed by  $T$ . Whenever ranks of adjacency submatrices are used, the field is  $\mathbb{F}_2$ .

**Treewidth.** A tree decomposition of a graph  $G = (V, E)$  is a pair  $(T, \mathcal{B})$  where  $T$  is a tree with vertex set  $V(T)$  and  $\mathcal{B} = (B_t)_{t \in V(T)}$  is a family of bags  $B_t \subseteq V$  satisfying the following conditions.

1. Every vertex appears in some bag:  $V = \bigcup_{t \in V(T)} B_t$ .
2. Every edge is covered by some bag: for every  $uv \in E$ , there is a node  $t$  with  $u, v \in B_t$ .
3. Bags containing a fixed vertex form a connected subtree: for every  $v \in V$ , the set  $\{t \in V(T) \mid v \in B_t\}$  is connected in  $T$ .

The width of  $(T, \mathcal{B})$  is  $\max_{t \in V(T)} |B_t| - 1$ . The treewidth of  $G$  is

$$\text{tw}(G) = \min_{(T, \mathcal{B})} \left( \max_{t \in V(T)} |B_t| - 1 \right),$$

where the min ranges over all tree decompositions of  $G$ . We use the standard facts that treewidth is monotone under taking minors and that  $\text{tw}(K_t) = t - 1$ . Computing treewidth exactly is **NP**-hard in general. However, for every fixed integer  $k$ , one can decide whether  $\text{tw}(G) \leq k$  and, if so, construct a tree decomposition of width at most  $k$  in polynomial time, indeed in linear time for fixed  $k$  [Bod96].

**Rank-width.** Let  $G = (V, E)$  be a graph. For  $X \subseteq V$ , define the cut-rank of  $X$  in  $G$  by

$$\rho_G(X) = \text{rank}_{\mathbb{F}_2} \mathbf{A}_G[X, V \setminus X].$$

A rank-decomposition of  $G$  is a pair  $(T, \mu)$  where  $T$  is a subcubic tree and  $\mu$  is a bijection from the leaves of  $T$  to  $V$ . Here, subcubic simply means that the maximal degree of a node in  $T$  is three.

Each edge  $e$  of  $T$  induces a bipartition, or cut, of  $V$ . Indeed, deleting  $e$  splits  $T$  into two connected components. The leaves in these two components correspond, through  $\mu$ , to two disjoint subsets  $X_e$  and  $\overline{X}_e$  of  $V$ . Thus,  $V = X_e \uplus \overline{X}_e$ , where  $\uplus$  denotes the disjoint union.

The width of an edge  $e$  in  $T$  is then  $\rho_G(X_e)$ , the width of the decomposition is the maximum width of its edges, and finally, the rank-width of  $G$  is

$$\text{rw}(G) = \min_{(T, \mu)} \max_{e \in E(T)} \rho_G(X_e),$$

where  $E(T)$  is edge set of  $T$ .

Fixed-width rank decompositions can be found, if they exist, in polynomial time for each fixed width [iOS06, HiO08, iO17].

Linear rank-width is the linear-layout analogue of rank-width. A linear layout of  $G$  is an ordering  $\pi = (v_1, \dots, v_n)$  of  $V$ . Its width is  $\max_{1 \leq i < n} \rho_G(\{v_1, \dots, v_i\})$ . The linear rank-width of  $G$  is

$$\text{lrw}(G) = \min_{\pi} \max_{1 \leq i < n} \rho_G(\{v_1, \dots, v_i\}).$$

Equivalently, it is rank-width restricted to caterpillar-shaped rank decompositions [iO17]. That is, when the decomposition tree  $T$  in the rank-decomposition  $(T, \mu)$  is restricted to be a caterpillar: a tree whose nonleaf vertices form a path. Hence

$$\text{rw}(G) \leq \text{lrw}(G).$$

The inequality can be strict on natural graph families. In particular, Adler and Kanté prove that the linear rank-width of a forest equals its pathwidth; complete binary trees therefore have bounded rank-width but linear rank-width growing with their height [AK15]. We will use this fact later to argue our new algorithm is provably better than previous approaches on some families of circuits.

## 2.2 Quantum circuits and gate sets

We recall quantum circuits and fix the elementary gate set on which we phrase our results. For an  $n$ -qubit system, the state space is  $(\mathbb{C}^2)^{\otimes n} \cong \mathbb{C}^{2^n}$ , with computational basis states  $|x\rangle = |x_1 \dots x_n\rangle$ ,  $x_i \in \{0, 1\}$ . A general  $n$ -qubit state is therefore  $|\psi\rangle = \sum_{x \in \{0,1\}^n} a_x |x\rangle$  with  $a_x \in \mathbb{C}$ , and for normalized states  $\sum_{x \in \{0,1\}^n} |a_x|^2 = 1$ . A quantum gate is a unitary linear operator acting on one or more qubits; when a gate acts on only a subset of the  $n$  qubits, it is understood to act as the identity on the remaining ones. A quantum circuit is a finite sequence of such gates acting on a fixed number of qubits.

**Elementary gate set.** The circuits we consider are built over the set of elementary gates  $\{\text{H}, \text{T}, \text{CZ}\}$ , with standard matrices

$$\text{H} = \frac{1}{\sqrt{2}} \begin{bmatrix} 1 & 1 \\ 1 & -1 \end{bmatrix}, \quad \text{T} = \begin{bmatrix} 1 & 0 \\ 0 & e^{i\pi/4} \end{bmatrix}, \quad \text{CZ} = \begin{bmatrix} 1 & 0 & 0 & 0 \\ 0 & 1 & 0 & 0 \\ 0 & 0 & 1 & 0 \\ 0 & 0 & 0 & -1 \end{bmatrix}.$$

The gate set  $\{\text{H}, \text{T}, \text{CZ}\}$  is universal for quantum computation and is also known as the Clifford + T gate set [NC10], where we note that the T gate renders one Clifford gate, namely  $\text{S} = \text{T}^2$ , redundant.

**Circuits.** We write an  $n$ -qubit circuit as

$$C = U_m \cdots U_2 U_1,$$

where the gates are ordered as applied:  $U_1$  first, then  $U_2$ , and so on up to  $U_m$ . We refer to the index  $i$  as the *position* of the gate  $U_i$  in the circuit. The action of  $C$  on an input state  $|\psi\rangle$  is  $C|\psi\rangle = U_m \cdots U_2 U_1 |\psi\rangle$ , and the matrix of the

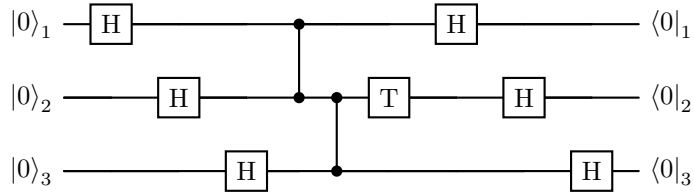


Figure 1: Running example: a 3-qubit circuit  $C$  over  $\{H, T, CZ\}$ , with the all-zeros input and output basis states pinned.

whole circuit is obtained by multiplying the gate matrices in reverse textual order, since the rightmost gate acts first.

To specify which qubits a gate acts on, we use the standard subscript convention:  $H_a$  and  $T_a$  denote a single-qubit Hadamard or T gate applied to qubit  $a$  (and the identity on every other wire), and  $CZ_{a,b}$  denotes a CZ gate applied to qubits  $a$  and  $b$  (and the identity elsewhere); since CZ is symmetric in its two arguments, the order of  $a$  and  $b$  does not matter. For a qubit  $a$ , the *Hadamard depth*  $k_a$  is the total number of H gates that act on qubit  $a$  in  $C$ . This count indexes the path variables on wire  $a$  in the sum-of-powers construction of [Section 3](#).

**Strong simulation.** Throughout the paper, by classical *strong simulation* of a circuit  $C$  we mean the task of computing, for given input and output computational basis states  $|\mathbf{y}\rangle$  and  $|\mathbf{z}\rangle$  with  $\mathbf{y}, \mathbf{z} \in \{0, 1\}^n$ , the amplitude

$$\langle \mathbf{z} | C | \mathbf{y} \rangle \in \mathbb{C},$$

i.e. the entry of the unitary associated with  $C$  in row  $\mathbf{z}$  and column  $\mathbf{y}$ . This is the quantity whose squared modulus  $|\langle \mathbf{z} | C | \mathbf{y} \rangle|^2$  is the probability of observing outcome  $\mathbf{z}$  when  $C$  is run on input  $\mathbf{y}$  and measured in the computational basis. Strong simulation is therefore strictly more demanding than weak simulation, which only requires producing samples from this output distribution.

**Example 1** (Running circuit). We illustrate the constructions of this paper using the 3-qubit circuit  $C$  shown in [Figure 1](#): an initial layer of H on every qubit (positions 1–3), then  $CZ_{1,2}$  and  $CZ_{2,3}$  (positions 4, 5), a single T on qubit 2 (position 6), and a final layer of H on every qubit (positions 7–9). Six H gates, one T, and two CZ’s give nine gates total. Our running target is the amplitude  $\langle 000 | C | 000 \rangle$ .

### 2.3 Tensor networks

The standard route to strong simulation contracts the circuit’s tensor network, and we will measure our SOP-based algorithm against it ([Section 3.2](#)); we therefore recall tensor networks and the contraction complexity that governs their cost.

A *tensor* of order  $k$  is a multilinear map  $A: [d_1] \times \cdots \times [d_k] \rightarrow \mathbb{C}$ , where  $[d] = \{0, \dots, d-1\}$ ; each of the  $k$  argument positions is an *index*, and we write  $A[a_1, \dots, a_k]$  for the entry of  $A$  at  $(a_1, \dots, a_k)$ . A *tensor network* is a finite collection of tensors  $\mathcal{T} = \{A_1, \dots, A_m\}$  together with a pairing of some

of their index positions across different tensors. Each matched pair (whose two positions must share a dimension) is a single *bond* (or *contracted index*), and the unmatched positions are the *open* (or *free indices*); write  $b_1, \dots, b_p$  for the bond indices and  $o_1, \dots, o_\ell$  for the open ones.

A *bond configuration*  $\beta = (\beta_1, \dots, \beta_p)$  assigns a value  $\beta_i \in [d_{b_i}]$  to every bond index  $b_i$ . Together with a choice  $\mathbf{j} = (j_1, \dots, j_\ell)$  of values for the open indices, it fixes a value for *every* index position of *every* tensor, so each  $A_t$  has a well-defined entry. The *value* of the network is the order- $\ell$  tensor obtained by summing, over all bond configurations, the product of these entries:

$$V[j_1, \dots, j_\ell] = \sum_{\beta_1, \dots, \beta_p} \prod_{t=1}^m A_t[\beta, \mathbf{j}],$$

where  $A_t[\beta, \mathbf{j}]$  denotes the entry of  $A_t$  read at the values that  $(\beta, \mathbf{j})$  assigns to the indices of  $A_t$ . For circuits every index is a qubit wire, so each dimension is  $d = 2$ .

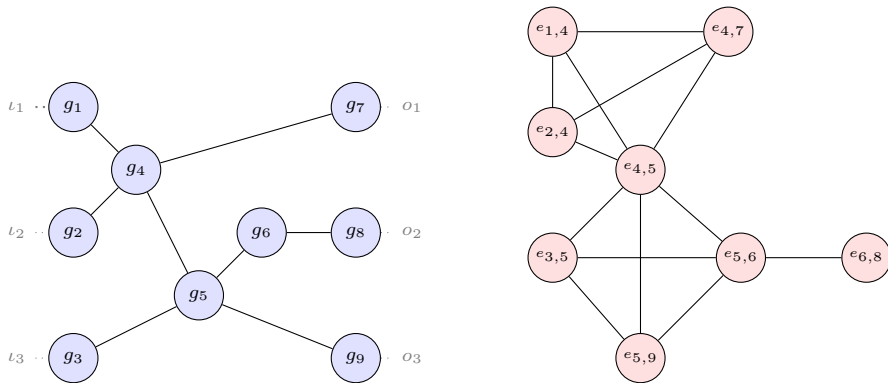
**Tensor-network graph.** Given a tensor network  $\mathcal{T}$ , its *tensor-network graph* (a multigraph)  $N_{\mathcal{T}}$  has one vertex per tensor and one edge  $\{t, t'\}$  for each bond index shared between  $A_t$  and  $A_{t'}$ ; open indices are not represented by edges.

It is sometimes convenient to represent a quantum circuit  $C = U_m \cdots U_1$  over  $\{\text{H, T, CZ}\}$  as a tensor network. In this context, each gate is a tensor: H and T are order-2 tensors (one input, one output qubit index) and CZ is order-4 (two input, two output qubit indices). Adjacent gates sharing a wire are connected by a bond index; the circuit's input and output wires are the open indices. The tensor-network graph  $N_C$  thus has one vertex per gate and one edge per wire segment connecting two gates.

**Example 2** (Deriving  $N_C$ ). The circuit of [Example 1](#) has nine gate tensors  $g_1, \dots, g_9$ , one for each gate in left-to-right order. Each H and T gate contributes a rank-2 tensor, with one input index and one output index, while each CZ gate contributes a rank-4 tensor, with two input indices and two output indices. We define  $N_C = (V, E)$  by taking  $V$  to be the set of gate tensors and  $E$  to be the set of internal bonds, that is, the wire segments connecting consecutive gates on the same qubit wire. In [Figure 2a](#), the eight such internal bonds are drawn as the eight edges of  $N_C$ .

The input and output indices are not edges of  $N_C$ . They are boundary indices, handled separately by the boundary assignment  $(\mathbf{y}, \mathbf{z})$  when considering the pinned amplitude  $\langle \mathbf{z} | C | \mathbf{y} \rangle$ . Equivalently, one may obtain a fully contracted network for this amplitude by adjoining rank-1 boundary tensors, which fix the input values  $\mathbf{y}$  and project onto the output values  $\mathbf{z}$ . In [Figure 2a](#), these boundary indices are shown for completeness as dotted open legs.

**Contraction complexity.** A *contraction order* is a sequence of pairwise tensor contractions that reduces the network to a single tensor. A contraction step merges two tensors and sums out their shared indices, producing a new tensor whose bond indices with the rest of the network are the union of those of the two; its cost is exponential in the number of indices of this intermediate tensor. This process is captured by the *line graph*  $L(N_C)$ , whose vertices are the bond



(a) The tensor-network graph  $N_C$  for the circuit of [Example 1](#). Solid edges are bond indices (wire segments between consecutive gates); dotted edges are boundary indices.

(b) The line graph  $L(N_C)$  for the circuit of [Example 1](#). Note how bond indices become exactly the vertex set. In particular, there are no (open) boundary vertices.

Figure 2: A tensor-network graph and its corresponding line graph.

indices of  $N_C$  (its edges) and whose edges record co-occurrence in a common tensor: a contraction step corresponds exactly to a vertex-elimination step, in which the shared indices are removed and the remaining indices on the merged tensor form a clique. A full contraction order is therefore an elimination order on  $L(N_C)$ , and Markov and Shi [[MS08](#)] showed that the minimum-cost order is governed by  $\text{tw}(L(N_C))$ . This motivates the definition

$$\text{cc}(N_C) := \text{tw}(L(N_C))$$

of the contraction complexity of a circuit.

**Example 3** (Deriving  $L(N_C)$ ). Continuing [Example 2](#), each tensor of  $N_C$  contributes a clique on its incident bond indices in  $L(N_C)$ . The two CZ's have all four of their indices internal, so each gives a  $K_4$ :  $\{e_{1,4}, e_{4,7}, e_{2,4}, e_{4,5}\}$  from  $g_4 = \text{CZ}_{1,2}$  and  $\{e_{4,5}, e_{5,6}, e_{3,5}, e_{5,9}\}$  from  $g_5 = \text{CZ}_{2,3}$ , sharing the bond index  $e_{4,5}$  on the wire of qubit 2 between them. The T at position 6 has two bond indices and so contributes the single edge  $e_{5,6} - e_{6,8}$ . Each of the six boundary Hadamards has only one bond index—its other index is an open input/output index—and so contributes no edge; these open indices are the leaves omitted from the bond-restricted  $L(N_C)$  of [Figure 2b](#).

### 3 Quadratic sums-of-powers for circuits

In [Section 2.2](#), we defined strong simulation as the task of evaluating the amplitude  $\langle z|C|y \rangle$ . We now recall how, for circuits over  $\{\text{H}, \text{T}, \text{CZ}\}$ , this amplitude is a quadratic *sum-of-powers* (SOP): a scalar sum of roots of unity over Feynman paths [[DHM+05](#), [WCYJ25](#), [CWD+25](#)]. The SOP, and the graph  $G_C$  it induces on its variables, are the central objects of the paper. After deriving them, we show in [Section 3.2](#) that  $G_C$  is never more complex than the circuit's tensor network, so already at this stage SOP evaluation is competitive with

tensor-network contraction; the rank-width refinement that beats it comes in [Section 4](#).

### 3.1 Sum of powers form and associated graph

For a circuit  $C = U_m \cdots U_1$ , inserting computational-basis resolutions of the identity between consecutive gates gives

$$\langle z|C|\mathbf{y}\rangle = \sum_{\mathbf{y}_1, \dots, \mathbf{y}_{m-1}} \prod_{j=1}^m \langle \mathbf{y}_j | U_j | \mathbf{y}_{j-1} \rangle, \text{ where } \mathbf{y}_0 = \mathbf{y} \text{ and } \mathbf{y}_m = \mathbf{z}.$$

**Local gate factors.** For the gate set  $\{\text{H}, \text{T}, \text{CZ}\}$ , every nonzero local matrix entry is a power of  $\omega_8 = e^{2\pi i/8}$ , up to the  $1/\sqrt{2}$  normalization carried by each Hadamard. For  $p, q, p_1, p_2, q_1, q_2 \in \{0, 1\}$ ,

$$\begin{aligned} \langle p|\text{H}|q\rangle &= 2^{-1/2}(-1)^{pq} = 2^{-1/2}\omega_8^{4pq}, \\ \langle p|\text{T}|q\rangle &= \delta_{p,q}\omega_8^p, \text{ and} \\ \langle p_1 p_2 | \text{CZ} | q_1 q_2 \rangle &= \delta_{p_1, q_1} \delta_{p_2, q_2} \omega_8^{4p_1 p_2}. \end{aligned} \tag{1}$$

Thus a Hadamard contributes a quadratic phase  $4pq$  together with a factor  $1/\sqrt{2}$ ; a T-gate contributes a unary phase  $p$ ; and a CZ-gate contributes a quadratic phase  $4p_1 p_2$ . All exponents are taken modulo 8.

**Path variables.** The Kronecker deltas in the T and CZ entries (see [Equation 1](#)) force each summand to vanish unless the value on every affected wire is unchanged across the gate, so the incoming and outgoing indices across such a diagonal gate may be identified. A Hadamard has no such delta, so the values immediately before and after it remain independent. Equivalently, cut each qubit wire at every Hadamard: on wire  $a$  this yields  $k_a + 1$  maximal segments, where  $k_a$  is the number of Hadamards on wire  $a$ , carrying Boolean variables  $x_{a,0}, \dots, x_{a,k_a}$ . Writing  $S$  for the set of all segment variables and reading off the contributions above,

- a T-gate on segment  $s$  contributes  $x_s$ ;
- a CZ-gate touching segments  $s, t$  contributes  $4x_s x_t$ ;
- a Hadamard from segment  $s$  to its successor  $s'$  contributes  $4x_s x_{s'}$  and one factor  $1/\sqrt{2}$ .

Summing these local exponents gives a raw quadratic phase polynomial

$$f(\mathbf{x}) = \sum_{\text{T on } s} x_s + 4 \sum_{\text{H: } s \rightarrow s'} x_s x_{s'} + 4 \sum_{\text{CZ on } s, t} x_s x_t \pmod{8},$$

with all sums counted with multiplicity and all coefficients reduced modulo 8.

**Pinning the boundary.** To compute  $\langle z|C|\mathbf{y}\rangle$  we impose the boundary conditions on  $f$ . Let  $s_{\text{in}}(a)$  and  $s_{\text{out}}(a)$  be the first and last segments on wire  $a$ , and pin  $x_{s_{\text{in}}(a)} = y_a$  and  $x_{s_{\text{out}}(a)} = z_a$  for  $a = 1, \dots, n$ . If these substitutions assign two different values to the same segment variable, then no Feynman path is compatible with the boundary data and  $\langle z|C|\mathbf{y}\rangle = 0$ . Otherwise, let  $V \subseteq S$  be the set of unpinned segment variables and write  $f|_{\mathbf{y}, \mathbf{z}}$  for the polynomial obtained from  $f$  after substituting the pinned variables.

**The pinned SOP.** Collecting terms in  $f|_{\mathbf{y},\mathbf{z}}$ , the constant terms combine into a single phase  $c \in \mathbb{Z}_8$ , the surviving one-variable terms become coefficients  $b_v \in \mathbb{Z}_8$  (the T-gate phases together with any sign interaction having exactly one pinned endpoint), and the surviving free–free quadratic interactions become the edges  $E$  of a graph on the unpinned variables  $V$ . Writing  $f_C := f|_{\mathbf{y},\mathbf{z}}$ ,

$$f_C(\mathbf{x}) = c + \sum_{v \in V} b_v x_v + 4 \sum_{\{u,v\} \in E} x_u x_v \pmod{8},$$

$$\langle \mathbf{z} | C | \mathbf{y} \rangle = \frac{1}{R} \sum_{\mathbf{x} \in \{0,1\}^V} \omega_8^{f_C(\mathbf{x})},$$

with  $R = (\sqrt{2})^{m_H}$  and  $m_H$  the number of Hadamards in  $C$ . We call  $G_C = (V, E)$  the *SOP variable graph* of the pinned amplitude  $(C, \mathbf{y}, \mathbf{z})$ .

**General quadratic SOP.** We now state the SOP and its associated counting problem in their general form, decoupled from any particular circuit. Let  $G = (V, E)$  be a graph,  $r$  an even positive integer,  $c \in \mathbb{Z}_r$ , and  $b_v \in \mathbb{Z}_r$  for every  $v \in V$ . Consider the quadratic SOP

$$Z = \frac{1}{R} \sum_{\mathbf{x} \in \{0,1\}^V} \omega_r^{f(\mathbf{x})}, \text{ with} \tag{2}$$

$$f(\mathbf{x}) = c + \sum_{v \in V} b_v x_v + \eta \sum_{\{u,v\} \in E} x_u x_v \pmod{r},$$

where  $\omega_r$  is the  $r$ th root of unity. Throughout the paper the edge coefficient is fixed as  $\eta = r/2$ ; this is the value produced by the construction above for  $\{\text{H, T, CZ}\}$  (where  $r = 8$  and  $\eta = 4$ ), and is what makes each cross-term contribute only a sign  $(-1)^{x_u x_v}$ .

**Definition 1 (Quadratic SopCount).** *Given an even integer  $r$ , a graph  $G = (V, E)$ , and a polynomial  $f$  as in Equation 2, the problem **SopCount** asks for all counts*

$$N_j = \#\{\mathbf{x} \in \{0,1\}^V \mid f(\mathbf{x}) = j \pmod{r}\}, \quad j \in \mathbb{Z}_r.$$

The SOP value is then recovered via

$$Z = \frac{1}{R} \sum_{j=0}^{r-1} N_j \omega_r^j.$$

For a circuit over  $\{\text{H, T, CZ}\}$  this is the instance with  $r = 8$  and  $G = G_C$ , the coefficients  $b_v$  and constant  $c$  being those identified above.

**Example 4 (Deriving  $G_C$ ).** Continuing Example 1, cutting each wire at its Hadamards yields one segment variable per wire segment. Since each qubit has Hadamard depth  $k_a = 2$ , every wire contributes three variables  $x_{a,0}, x_{a,1}, x_{a,2}$ , with  $x_{a,0}$  and  $x_{a,2}$  fixed by the input and output basis states. Pinning  $|000\rangle \rightarrow |000\rangle$  therefore leaves  $V = \{x_{1,1}, x_{2,1}, x_{3,1}\}$  as the only free variables. Quadratic cross-terms come from the two CZ gates: CZ<sub>1,2</sub> acts on  $x_{1,1}$  and  $x_{2,1}$  (the current variables on the two wires at position 4), and CZ<sub>2,3</sub> acts on  $x_{2,1}$  and  $x_{3,1}$ . Each

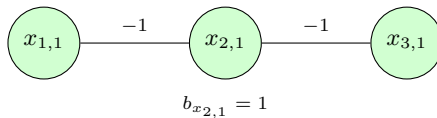


Figure 3: The SOP variable graph  $G_C$  for the circuit  $C$  of [Example 1](#) after pinning  $|000\rangle \rightarrow |000\rangle$ . Every edge carries the constant cross-term sign  $\omega_8^4 = -1$ , contributed as  $(-1)^{x_u x_v}$ . Vertices carry unary phases  $\omega_8^{b_v}$ : the only nontrivial one here is  $b_{x_{2,1}} = 1$  (from the T gate), giving the phase  $\omega_8 = e^{i\pi/4}$  at  $x_{2,1} = 1$ .

such edge carries the constant cross-term sign  $\omega_8^4 = -1$ , contributed as  $(-1)^{x_u x_v}$ . The T on qubit 2 at position 6 contributes the unary phase coefficient  $b_{x_{2,1}} = 1$ , so the phase at  $x_{2,1} = 1$  is  $e^{i\pi/4} = \omega_8$ . The resulting SOP variable graph  $G_C$  is the path of [Figure 3](#).

### 3.2 SOP evaluation matches contraction complexity

Recall from [Section 2.3](#) the tensor-network graph  $N_C$  of a circuit, its line graph  $L(N_C)$ , and the contraction complexity  $\text{cc}(N_C) = \text{tw}(L(N_C))$  governing the Markov–Shi tensor-contraction bound [[MS08](#)]. We relate the SOP variable graph  $G_C$  of [Section 3](#) to this quantity. The resulting bound  $\text{tw}(G_C) \leq \text{cc}(N_C)$  lets us compare the rank-width FPT dynamic program of [Section 4](#) with tensor contraction ([Section 5](#)), and it yields a treewidth FPT dynamic program for SOP evaluation directly, as explained below.

**Lemma 1** (SOP graph is a minor of the tensor line graph). *For circuits  $C$  over  $\{\text{H}, \text{T}, \text{CZ}\}$ , the SOP variable graph  $G_C$  is a minor of  $L(N_C)$ . Consequently  $\text{tw}(G_C) \leq \text{tw}(L(N_C)) = \text{cc}(N_C)$ .*

*Proof.* We must show that  $G_C$  is a minor of  $L(N_C)$ , i.e. that it arises from  $L(N_C)$  by vertex deletions and edge contractions. The announced bound  $\text{tw}(G_C) \leq \text{tw}(L(N_C)) = \text{cc}(N_C)$  then follows by minor-monotonicity of treewidth.

Recall the differences between the two graphs: The vertices of  $L(N_C)$  are the bond indices of the tensor-network representation of  $C$  (the wire segments between consecutive gates), with two of them being adjacent when they occur on a common gate tensor. The vertices of  $G_C$  are the *free* segment variables  $x_{a,j}$  of [Section 3](#). We go from the first graph to the second in three steps.

*Step 1 (collapse each wire sector).* Group the bonds of  $N_C$  by the maximal stretch of a wire that contains them: two bonds lie in the same stretch when no Hadamard separates them, with the wire’s input and output legs as its outer boundaries. Inside a stretch every gate is diagonal, that is, a T gate, or one leg of a CZ, and so they leave the wire value unchanged ([Section 3](#)). The stretch’s bonds therefore carry a common value and form a connected path in  $L(N_C)$ , consecutive ones being adjacent through the diagonal gate between them. Contracting this path to a single vertex yields one vertex per stretch that contains a bond. A stretch lying strictly between two Hadamards always contains a bond, and its vertex is the free segment variable  $x_{a,j}$ .

*Step 2 (delete the pinned segments).* The two outer stretches of each wire, i.e. before its first Hadamard and after its last, carry the pinned values  $y_a$  and  $z_a$ . Their open input/output indices are not vertices of  $L(N_C)$  at all, since open

indices are not edges of  $N_C$ ; the only vertex an outer stretch can contribute is one formed in Step 1 from bonds lying outside the wire’s outermost Hadamards. We delete any such vertex, folding its contribution into the coefficients  $b_v$  and the constant  $c$  as in Section 3. In particular, when a wire begins and ends with a Hadamard, like every wire of Example 1 does, its outer stretches contain no bond and nothing is deleted. The remaining vertices are the free segment variables, so exactly the vertex set  $V$  of  $G_C$ .

*Step 3 (match the edges).* It remains to verify that the adjacencies left by Steps 1–2 are exactly the edges  $E$  of  $G_C$ . A CZ gate on wires  $a, b$  has its two relevant indices on the same tensor, hence adjacent in  $L(N_C)$ . After the contractions of Step 1 these become the two segment vertices the gate acts on, giving the cross-term edge  $\{x_{a,j_a}, x_{b,j_b}\}$ . An *interior* Hadamard—one both of whose incident indices are non-boundary—likewise has those two indices on a common tensor, contributing the edge between the segment variable before it and the fresh one after it. A Hadamard at the start or end of a wire instead has one incident index in an outer stretch (either an open leg, which is not in  $L(N_C)$ , or a bond removed in Step 2) so only its inner segment vertex survives and it contributes no edge. No other gate creates an adjacency between free variables, so the surviving adjacencies are exactly  $E$ .  $\square$

Since we only have fixed-arity tensor networks (that arise from quantum circuits) one may also compare to the treewidth of  $N_C$  itself [MS08]. If every tensor has arity at most  $\Delta$ , then a tree decomposition of  $N_C$  of width  $t$  can be converted into one of  $L(N_C)$  of width at most  $\Delta(t + 1) - 1$  by replacing each bag with all incident tensor indices. Without bounded arity, this implication is false: a star with one high-arity tensor has treewidth one as a tensor graph, but a line graph that is a clique.

Thus  $\text{tw}(G_C) \leq \text{cc}(N_C)$ : the SOP variable graph is never harder than the tensor-network contraction. Quadratic SOP evaluation is moreover a special case of the standard sum–product problem on a graphical model: the variables are Boolean and the unary and binary factors are exactly the coefficients of Equation 2, so the SOP variable graph  $G_C$  is the *primal graph* of the instance. By bucket elimination (equivalently, tree-decomposition dynamic programming) such instances can be evaluated in time  $2^{O(\text{tw}(G_C))} \text{poly}(n)$  [Dec99, GKSS22]. The link between path-sum formulas and graphical-model primal graphs is also noted in [CWD<sup>+</sup>25]; here Lemma 1, together with the observation that  $G_C$  is the primal graph, lets us invoke this framework directly to obtain a treewidth FPT dynamic program for SOP evaluation that already matches the Markov–Shi contraction-complexity guarantee. Section 4 refines the parameter from treewidth to the rank-width of  $G_C$ .

## 4 Rank-based dynamic program for SOPs

This section gives the paper’s main algorithm: an exact evaluation of a quadratic SOP that is fixed-parameter tractable in the *rank-width* of its variable graph  $G_C$ . Since rank-width can be much smaller than treewidth or linear rank-width, this is what lets the SOP route outperform both tensor contraction and decision-diagram simulators on the circuit families of Section 5. We give a dynamic-programming algorithm that processes a rooted rank-decomposition

$(\mathcal{T}, \mu)$  of  $G_C$  from the leaves to the root in Section 4.1. Then, in Section 4.2 we propose an optimization based on Fourier-modes.

#### 4.1 SOP evaluation by rank-decomposition

The algorithm processes a rank-decomposition of  $G_C$  from the leaves upward, keeping at each node a compact table that records how the partial assignments below it interact with the rest of the graph. Because each cut of a width- $k$  decomposition has rank at most  $k$ , only  $2^k$  interaction patterns can occur, so the tables stay small—this is the source of the fixed-parameter guarantee.

**Setup.** We work with a rooted rank-decomposition  $(\mathcal{T}, \mu)$  of  $G_C$ :  $\mathcal{T}$  is a tree of maximum degree 3 whose leaves are in bijection with  $V$  via  $\mu$ , with one designated internal node  $r_{\mathcal{T}}$  as the *root* (obtained, if necessary, by subdividing an arbitrary edge of  $\mathcal{T}$  into an unrooted decomposition and rooting at the new vertex). For a node  $u$  of  $\mathcal{T}$ , let  $X_u \subseteq V$  be the set of vertices corresponding to leaves of the subtree rooted at  $u$ , and let  $\bar{X}_u = V \setminus X_u$ . At the root,  $X_{r_{\mathcal{T}}} = V$  and  $\bar{X}_{r_{\mathcal{T}}} = \emptyset$ ; at a leaf  $u$  with  $\mu(u) = v$ ,  $X_u = \{v\}$ . At each node  $u$ , the DP table records how assignments inside  $X_u$  look to the outside.

For  $\mathbf{z} \in \{0, 1\}^{X_u}$ , define the boundary signature

$$\sigma_u(\mathbf{z}) = \mathbf{z}^\top \mathbf{A}[X_u, \bar{X}_u] \in \mathbb{F}_2^{\bar{X}_u}.$$

This vector records, for each outside vertex, the parity of its selected neighbors inside  $X_u$ . Define the internal residue

$$\phi_u(\mathbf{z}) = \sum_{v \in X_u} b_v z_v + \eta \sum_{\{v, w\} \in E, v, w \in X_u} z_v z_w \pmod{r}.$$

The constant  $c$  is not included in  $\phi_u$  and is added back at the root.

The table at node  $u$  is stored sparsely. Its keys are pairs  $(\boldsymbol{\sigma}, s)$ , where  $s \in \mathbb{Z}_r$  and  $\boldsymbol{\sigma}$  is an occurring boundary signature, and it stores

$$D_u[\boldsymbol{\sigma}, s] = \#\{\mathbf{z} \in \{0, 1\}^{X_u} \mid \sigma_u(\mathbf{z}) = \boldsymbol{\sigma}, \phi_u(\mathbf{z}) = s\}.$$

Although  $\sigma_u(\mathbf{z})$  is written as a vector in  $\mathbb{F}_2^{\bar{X}_u}$ , it always lies in the image of the linear map

$$\{0, 1\}^{X_u} \rightarrow \mathbb{F}_2^{\bar{X}_u}, \quad \mathbf{z} \mapsto \mathbf{z}^\top \mathbf{A}[X_u, \bar{X}_u],$$

namely the row space of  $\mathbf{A}[X_u, \bar{X}_u]$  over  $\mathbb{F}_2$ . For every nonroot node  $u$ , the edge from  $u$  to its parent in the rooted rank-decomposition induces the cut  $(X_u, \bar{X}_u)$ . Since the decomposition has width  $k$ ,  $\text{rank}_{\mathbb{F}_2} \mathbf{A}[X_u, \bar{X}_u] \leq k$  and therefore at most  $2^k$  boundary signatures can occur at  $u$ . At the root,  $\bar{X}_u = \emptyset$ , so there is only the empty signature. Thus each table has at most  $r2^k$  nonzero states.

**Leaves.** If  $u$  is a leaf corresponding to vertex  $v$ , then  $X_u = \{v\}$ . The assignment  $z_v = 0$  contributes

$$D_u[0, 0] += 1,$$

and the assignment  $z_v = 1$  contributes

$$D_u[\mathbf{A}[v, V \setminus \{v\}], b_v] += 1.$$

The use of  $+=$  matters: the two states may coincide.

**Joins.** Let  $t$  be an internal node with children  $L$  and  $R$ . Write

$$X_t = X_L \uplus X_R, \quad Y = \overline{X}_t = V \setminus X_t.$$

Then  $\overline{X}_L = X_R \cup Y$  and  $\overline{X}_R = X_L \cup Y$ . Take a left state  $(\boldsymbol{\alpha}, p)$  and a right state  $(\boldsymbol{\beta}, q)$ , with

$$\boldsymbol{\alpha} \in \mathbb{F}_2^{X_R \cup Y}, \quad \boldsymbol{\beta} \in \mathbb{F}_2^{X_L \cup Y}.$$

Let  $\mathbf{a} \in \{0, 1\}^{X_L}$  and  $\mathbf{b} \in \{0, 1\}^{X_R}$  realize these states. The new quadratic terms are exactly the edges between  $X_L$  and  $X_R$ . Their parity is

$$\chi(\boldsymbol{\alpha}, \boldsymbol{\beta}) = \mathbf{a}^\top \mathbf{A}[X_L, X_R] \mathbf{b} \in \mathbb{F}_2.$$

This value is well-defined.

**Lemma 2.** *The value  $\chi(\boldsymbol{\alpha}, \boldsymbol{\beta})$  depends only on the signatures  $\boldsymbol{\alpha}$  and  $\boldsymbol{\beta}$ , and not on the chosen assignments  $\mathbf{a}$  and  $\mathbf{b}$  realizing them.*

*Proof.* Suppose  $\mathbf{a}'$  is another assignment in  $\{0, 1\}^{X_L}$  with the same left signature:  $\sigma_L(\mathbf{a}') = \sigma_L(\mathbf{a}) = \boldsymbol{\alpha}$ . Then, over  $\mathbb{F}_2$ ,

$$(\mathbf{a} - \mathbf{a}')^\top \mathbf{A}[X_L, V \setminus X_L] = \mathbf{0}.$$

Since  $X_R \subseteq V \setminus X_L$ , restricting this equality to the coordinates indexed by  $X_R$  gives

$$(\mathbf{a} - \mathbf{a}')^\top \mathbf{A}[X_L, X_R] = \mathbf{0}.$$

Multiplying by  $\mathbf{b}$  yields

$$\mathbf{a}^\top \mathbf{A}[X_L, X_R] \mathbf{b} = \mathbf{a}'^\top \mathbf{A}[X_L, X_R] \mathbf{b}.$$

Thus changing the left representative does not change the cross term.

The same argument applies on the right. If  $\mathbf{b}'$  satisfies  $\sigma_R(\mathbf{b}') = \sigma_R(\mathbf{b}) = \boldsymbol{\beta}$ , then

$$(\mathbf{b} - \mathbf{b}')^\top \mathbf{A}[X_R, V \setminus X_R] = \mathbf{0}.$$

Since  $X_L \subseteq V \setminus X_R$  and  $\mathbf{A}$  is symmetric, this implies

$$\mathbf{A}[X_L, X_R](\mathbf{b} - \mathbf{b}') = \mathbf{0}.$$

Therefore

$$\mathbf{a}^\top \mathbf{A}[X_L, X_R] \mathbf{b} = \mathbf{a}^\top \mathbf{A}[X_L, X_R] \mathbf{b}'.$$

The value  $\chi(\boldsymbol{\alpha}, \boldsymbol{\beta})$  is independent of all choices of representatives.  $\square$

The parent signature and residue are

$$\boldsymbol{\gamma} = \boldsymbol{\alpha}|_Y + \boldsymbol{\beta}|_Y \in \mathbb{F}_2^Y, \quad s = p + q + \eta\chi(\boldsymbol{\alpha}, \boldsymbol{\beta}) \pmod{r}.$$

The join does not create an unbounded set of parent signatures. If  $\boldsymbol{\alpha}$  and  $\boldsymbol{\beta}$  are realized by assignments  $\mathbf{a} \in \{0, 1\}^{X_L}$  and  $\mathbf{b} \in \{0, 1\}^{X_R}$ , then

$$\boldsymbol{\gamma} = \mathbf{a}^\top \mathbf{A}[X_L, Y] + \mathbf{b}^\top \mathbf{A}[X_R, Y] = (\mathbf{a}, \mathbf{b})^\top \mathbf{A}[X_t, Y] = \sigma_t(\mathbf{a}, \mathbf{b}).$$

Thus, every parent signature produced by the join lies in the row space of  $\mathbf{A}[X_t, Y]$ . Since  $Y = \overline{X}_t$ , the cut  $(X_t, Y)$  is again a cut induced by an edge of the rooted rank-decomposition unless  $t$  is the root. Therefore this row space has size at most  $2^k$  at every nonroot internal node, and size 1 at the root.

The join update is

$$D_t[\boldsymbol{\gamma}, s] += D_L[\boldsymbol{\alpha}, p] D_R[\boldsymbol{\beta}, q].$$

---

**Algorithm 1** Rank-decomposition DP for quadratic **SopCount**.

---

**Input:** Quadratic SOP polynomial  $f(\mathbf{x}) = c + \sum_v b_v x_v + \eta \sum_{\{u,v\} \in E} x_u x_v$  and a rooted rank-decomposition of  $G = (V, E)$  of width  $k$ .

**Output:** Counts  $N_j$  for  $j \in \mathbb{Z}_r$ .

```

1: for each leaf  $u$  with vertex  $v$  do
2:    $D_u \leftarrow$  empty sparse table keyed by occurring pairs  $(\boldsymbol{\sigma}, s)$ 
3:    $D_u[0, 0] += 1$ 
4:    $D_u[\mathbf{A}[v, V \setminus \{v\}], b_v \bmod r] += 1$ 
5: end for
6: for each internal node  $t$  in post-order do
7:   Let  $L, R$  be the children of  $t$  and  $Y \leftarrow \bar{X}_t$ .
8:    $D_t \leftarrow$  empty sparse table keyed by occurring pairs  $(\boldsymbol{\sigma}, s)$ 
9:   for all  $(\boldsymbol{\alpha}, p)$  with  $D_L[\boldsymbol{\alpha}, p] > 0$  do
10:    for all  $(\boldsymbol{\beta}, q)$  with  $D_R[\boldsymbol{\beta}, q] > 0$  do
11:       $\boldsymbol{\gamma} \leftarrow \boldsymbol{\alpha}|_Y + \boldsymbol{\beta}|_Y$ 
12:       $\chi \leftarrow \chi(\boldsymbol{\alpha}, \boldsymbol{\beta})$ 
13:       $s \leftarrow (p + q + \eta\chi) \bmod r$ 
14:       $D_t[\boldsymbol{\gamma}, s] += D_L[\boldsymbol{\alpha}, p] \cdot D_R[\boldsymbol{\beta}, q]$ 
15:    end for
16:  end for
17: end for
18: return  $(D_{r_T}[\emptyset, j - c \bmod r])_{j \in \mathbb{Z}_r}$ 

```

---

**Theorem 1** (Correctness). *For every node  $u$ , signature  $\boldsymbol{\sigma}$ , and residue  $s$ ,*

$$D_u[\boldsymbol{\sigma}, s] = \#\{\mathbf{z} \in \{0, 1\}^{X_u} \mid \sigma_u(\mathbf{z}) = \boldsymbol{\sigma}, \phi_u(\mathbf{z}) = s\}.$$

Consequently [Algorithm 1](#) returns the counts  $N_j$ .

*Proof.* The proof is by induction over the rooted decomposition tree. The leaf case is exactly the two assignments  $z_v = 0$  and  $z_v = 1$ .

For the join step, every assignment to  $X_t$  decomposes uniquely as  $(\mathbf{a}, \mathbf{b})$  with  $\mathbf{a} \in \{0, 1\}^{X_L}$  and  $\mathbf{b} \in \{0, 1\}^{X_R}$ . The boundary signature satisfies

$$\sigma_t(\mathbf{a}, \mathbf{b}) = (\mathbf{a}, \mathbf{b})^\top \mathbf{A}[X_t, Y] = \mathbf{a}^\top \mathbf{A}[X_L, Y] + \mathbf{b}^\top \mathbf{A}[X_R, Y] = \boldsymbol{\alpha}|_Y + \boldsymbol{\beta}|_Y.$$

For the residue, the only terms not already counted inside the two children are edges crossing from  $X_L$  to  $X_R$ , and the integer count of such selected crossing edges satisfies  $m \bmod 2 = \mathbf{a}^\top \mathbf{A}[X_L, X_R] \mathbf{b}$ . Since  $\eta = r/2$ , we have  $\eta m \equiv \eta(m \bmod 2) \pmod{r}$  for every integer  $m$ , so

$$\phi_t(\mathbf{a}, \mathbf{b}) = \phi_L(\mathbf{a}) + \phi_R(\mathbf{b}) + \eta\chi(\boldsymbol{\alpha}, \boldsymbol{\beta}) \pmod{r}.$$

By [Lemma 2](#), this depends only on the two child states. The child variable sets are disjoint, so the number of pairs of assignments realizing the two child states is  $D_L[\boldsymbol{\alpha}, p] D_R[\boldsymbol{\beta}, q]$ . The join rule adds exactly this quantity to the correct parent state. Summing over all child-state pairs proves the invariant.

At the root  $X_{r_T} = V$  and  $\bar{X}_{r_T} = \emptyset$ . Also  $f(\mathbf{x}) = c + \phi_{r_T}(\mathbf{x}) \pmod{r}$ . Hence  $f(\mathbf{x}) = j$  iff  $\phi_{r_T}(\mathbf{x}) = j - c$ , and the returned vector is  $(N_j)_{j \in \mathbb{Z}_r}$ .  $\square$

**Theorem 2** (Rank-width algorithm for quadratic SOPs). *Given a quadratic SOP instance with variable graph  $G$  and a rank-decomposition of  $G$  of width  $k$ , all counts  $N_j$  can be computed in time  $O(nr^2 4^k \text{poly}(n))$  and space  $O(nr 2^k)$ , or working space  $O(r 2^k \text{depth}(T))$  if tables are discarded after use. For fixed  $r$ , this is  $2^{O(k)} \text{poly}(n)$ .*

*Proof.* For every nonroot node  $u$ , the cut  $(X_u, \overline{X}_u)$  is induced by the edge from  $u$  to its parent in the rooted rank-decomposition. Hence,  $\text{rank}_{\mathbb{F}_2} \mathbf{A}[X_u, \overline{X}_u] \leq k$ . The possible boundary signatures at  $u$  are exactly the image of the linear map

$$\mathbf{z} \mapsto \mathbf{z}^\top \mathbf{A}[X_u, \overline{X}_u],$$

so there are at most  $2^k$  of them. At the root there is only the empty signature. Since the tables are stored sparsely and have one residue coordinate in  $\mathbb{Z}_r$ , every node has at most  $r 2^k$  nonzero states.

A naive join scans all pairs of child states, at most  $r^2 4^k$  pairs. Each pair performs one parent update, and the restriction of signatures, their addition, and the precomputed cross term  $\chi$  cost only polynomial time in  $n$  using explicit bit-vector representations. There are  $O(n)$  nodes in the decomposition tree.  $\square$

**Corollary 1** (Linear rank-width). *Since  $\text{rw}(G) \leq \text{lrw}(G)$  for every graph (Section 2.1), Theorem 2 evaluates a quadratic SOP in time  $2^{O(k)} \text{poly}(n)$  whenever the linear rank-width of its variable graph is at most  $k$ . In particular, on SOP variable graphs this matches—without decision diagrams—the linear-rank-width simulation guarantee of [CWD<sup>+</sup> 25].*

## 4.2 Fourier-mode implementation

The residue table of the previous subsection carries an avoidable factor  $r$  in the join. We remove it by working with the discrete Fourier transform of the residue counts on  $\mathbb{Z}_r$ , bringing the running time to the  $O(nr 4^k \text{poly}(n) + r \log r)$  bound quoted in Section 6.

**Residue counts and their Fourier transform.** The vector of residue counts  $N = (N_0, N_1, \dots, N_{r-1})$  is a function on the cyclic group  $\mathbb{Z}_r$ . Using the characters  $\chi_a(j) = \omega_r^{aj}$  for  $a, j \in \mathbb{Z}_r$ , define the discrete Fourier transform

$$\widehat{N}(a) = \sum_{j=0}^{r-1} N_j \chi_a(j) = \sum_{j=0}^{r-1} N_j \omega_r^{aj}. \quad (3)$$

This is the usual finite Fourier transform; the same transform and its inverse underlie the fast Fourier transform [CT65]. Here the group is only  $\mathbb{Z}_r$ , but the same principle is useful in what follows: instead of storing coefficients indexed by residues, we store evaluations against the  $\chi_a$ .

Equation 3 is also exactly an amplitude evaluation. Grouping the assignments  $\mathbf{x}$  by their residue  $f(\mathbf{x}) \pmod{r}$  gives

$$\widehat{N}(a) = \sum_{j=0}^{r-1} \#\{\mathbf{x} \in \{0, 1\}^V \mid f(\mathbf{x}) = j \pmod{r}\} \omega_r^{aj} = \sum_{\mathbf{x} \in \{0, 1\}^V} \omega_r^{af(\mathbf{x})},$$

since every assignment  $\mathbf{x}$  contributes to exactly one residue class. In particular, the original SOP value satisfies  $\widehat{N}(1) = \sum_{\mathbf{x}} \omega_r^{f(\mathbf{x})} = RZ$ , so amplitude evaluation gives one Fourier coefficient and evaluating the scaled polynomials  $af$  for all  $a \in \mathbb{Z}_r$  gives all of them. By orthogonality of characters of  $\mathbb{Z}_r$ , the transform inverts as

$$N_t = \frac{1}{r} \sum_{a=0}^{r-1} \omega_r^{-at} \widehat{N}(a), \quad t \in \mathbb{Z}_r. \quad (4)$$

Computing all residue counts and computing all scaled amplitude evaluations are therefore equivalent up to an  $r$ -point Fourier transform, performed in  $O(r \log r)$  when  $r$  has a suitable factorization (and in  $O(r^2)$  by direct inversion otherwise — lower-order in the fixed- $r$  regime).

**Per-mode dynamic program.** This suggests running the rank-decomposition DP *one Fourier mode at a time*: for each  $a \in \mathbb{Z}_r$ , track only one complex number per boundary signature, computing  $\widehat{N}(a)$  in a single pass, and recover all  $N_j$  at the root via (4). Concretely, for each  $a \in \mathbb{Z}_r$  define

$$A_u^{(a)}[\boldsymbol{\sigma}] = \sum_{\substack{\mathbf{z} \in \{0,1\}^{X_u} \\ \sigma_u(\mathbf{z}) = \boldsymbol{\sigma}}} \omega_r^{a\phi_u(\mathbf{z})}.$$

At the root,

$$\widehat{N}(a) = \sum_{\mathbf{x} \in \{0,1\}^V} \omega_r^{af(\mathbf{x})} = \omega_r^{ac} A_{r\tau}^{(a)}[\emptyset],$$

and the counts are recovered by

$$N_j = \frac{1}{r} \sum_{a=0}^{r-1} \omega_r^{-aj} \widehat{N}(a) = \frac{1}{r} \sum_{a=0}^{r-1} \omega_r^{a(c-j)} A_{r\tau}^{(a)}[\emptyset]. \quad (5)$$

For a fixed mode  $a$ , the leaf initialization becomes

$$A_u^{(a)}[0] += 1, \quad A_u^{(a)}[\mathbf{A}[v, V \setminus \{v\}]] += \omega_r^{ab_v}.$$

At a join,

$$A_t^{(a)}[\boldsymbol{\gamma}] += A_L^{(a)}[\boldsymbol{\alpha}] A_R^{(a)}[\boldsymbol{\beta}] \omega_r^{a\eta\chi(\boldsymbol{\alpha}, \boldsymbol{\beta})}.$$

Since  $\eta = r/2$ ,

$$\omega_r^{a\eta\chi} = \omega_r^{a(r/2)\chi} = (-1)^{a\chi}.$$

Thus the interaction kernel depends only on the parity of  $a$ : even modes have no signed cross term, and odd modes have the same  $(-1)^\chi$  kernel.

**Theorem 3** (Fourier speedup). *Given a rank-decomposition of  $G$  of width  $k$ , all counts  $N_j$  of a quadratic SOP can be computed in time  $O(nr4^k \text{poly}(n) + r \log r)$ .*

*Proof.* For each fixed  $a \in \mathbb{Z}_r$ , the table has only one complex value per occurring boundary signature. As above, the occurring signatures at a nonroot node  $u$  form the row space of  $\mathbf{A}[X_u, \overline{X}_u]$ , whose dimension is at most  $k$ ; at the root there is only the empty signature. Hence each table has at most  $2^k$  states per node. The naive join scans at most  $4^k$  pairs of child signatures. Running this dynamic program for all  $r$  modes costs  $O(nr4^k \text{poly}(n))$ . The inverse transform Equation 5 costs  $O(r \log r)$  using an FFT when the coefficient field supports it, or  $O(r^2)$  by direct inversion if  $r$  is not treated as fixed.  $\square$

**Implementation details.** All of the Fourier modes share the same rank-decomposition, signature spaces, restriction maps, parent-signature maps, and cross-term table  $\chi(\alpha, \beta)$ . These maps can be precomputed once for each join node. The only mode-dependent leaf data are the unary phases  $\omega_r^{ab_v}$ , and the only mode-dependent join data are the two kernels given by the parity of  $a$ . In practice one therefore batches even modes and odd modes separately. The asymptotic bound remains  $O(nr4^k \text{poly}(n))$ , but the constant factors are smaller than in a literal execution of  $r$  independent programs.

## 5 Breaking through the linear rank-width and contraction complexity barriers

The dynamic program above is parameterized by the rank-width of the SOP variable graph. This is a branching parameter: the decomposition tree may split the variables recursively. Linear decision-diagram approaches [CWD<sup>+</sup>25] use a variable ordering and are therefore governed by a linear layout parameter, such as linear rank-width. Tensor-network contraction is governed by the contraction complexity  $\text{cc}(N_C) = \text{tw}(L(N_C))$ . The following construction separates these parameters at the level of the SOP variable graph, so the advantage of Section 4 is not an artifact of a particular benchmark but provable on explicit circuit families.

$$\begin{array}{ccccc}
 & & \text{general} & & \text{family } C_{h,t} \\
 & & & & O(1) \text{ vs } \geq t-1 \\
 \text{lrw}(G_C) & \geq & \text{rw}(G_C) & \leq & \text{tw}(G_C) \\
 & & \Rightarrow \text{cc}(N_C) = \Omega(t) \text{ by Lemma 1} & & 
 \end{array}$$

Figure 4: The three structural parameters governing the competing algorithmic routes: rank-width (rw, the dynamic program of this section), linear rank-width (lrw, linear decision-diagram approaches), and treewidth (tw, tensor contraction). The family  $C_{h,t}$  of Corollary 2 keeps  $\text{rw} = O(1)$  while  $\text{lrw} = \Omega(h)$  and  $\text{tw} \geq t - 1$  (hence  $\text{cc}(N_C) = \Omega(t)$  by Lemma 1).

We first establish that for an arbitrary simple graph we can construct a quantum circuit such that its SOP variable graph is the graph input graph. This avoids relying on a special feature of a particular benchmark family (cf. the separation from [CWD<sup>+</sup>25]).

**Lemma 3** (Realizing a graph as an SOP variable graph). *Let  $\Gamma = (W, F)$  be a simple graph. There is a circuit  $C_\Gamma$  over  $\{\text{H}, \text{CZ}\}$  with  $|W|$  qubits and  $2|W| + |F|$  gates such that, after fixing the input and output basis states and substituting the pinned variables, the SOP variable graph is exactly  $\Gamma$ .*

*Proof.* Use one qubit  $q_v$  for each vertex  $v \in W$ . Apply one H gate to every qubit, then for every edge  $\{u, v\} \in F$  apply one CZ gate between  $q_u$  and  $q_v$ , and finally apply one more H gate to every qubit.

For qubit  $q_v$  the two H gates create three qubit-time variables  $x_{v,0}, x_{v,1}, x_{v,2}$ . The variables  $x_{v,0}$  and  $x_{v,2}$  are fixed by the input and output basis states. Hence, after substituting these pinned values, they are constants. The two

H interactions on the wire contribute the factors  $(-1)^{x_{v,0}x_{v,1}}$  and  $(-1)^{x_{v,1}x_{v,2}}$ . Since  $x_{v,0}$  and  $x_{v,2}$  are fixed, these factors are unary phases in the remaining variable  $x_{v,1}$ . They do not create quadratic edges among the free variables.

Every CZ gate for an edge  $\{u, v\} \in F$  is placed between the two layers of H gates. At that time the current variables on the two wires are  $x_{u,1}$  and  $x_{v,1}$ , so the CZ gate contributes the quadratic factor  $(-1)^{x_{u,1}x_{v,1}}$ . Thus the remaining variables are precisely  $\{x_{v,1} : v \in W\}$ , and two such variables have a quadratic interaction if and only if the corresponding vertices of  $\Gamma$  are adjacent. The SOP variable graph is therefore  $\Gamma$ .  $\square$

We next define a family of graphs with bounded rank-width, unbounded linear rank-width, and arbitrarily large treewidth. Let  $B_h$  be the complete binary tree of height  $h$ . For an integer  $t \geq 1$ , let

$$\Gamma_{h,t} = B_h[K_t]$$

be the graph obtained from  $B_h$  by replacing every vertex  $v$  by a clique  $K_t^v$  of  $t$  twins, and by replacing every tree edge  $\{u, v\}$  by the complete bipartite graph between  $K_t^u$  and  $K_t^v$ . Equivalently,  $\Gamma_{h,t}$  is the lexicographic blow-up of  $B_h$  by a  $t$ -clique.

**Lemma 4.** *For all  $h$  and  $t \geq 1$ ,*

- $\text{rw}(\Gamma_{h,t}) = O(1)$ ,
- $\text{lrw}(\Gamma_{h,t}) = \Omega(h)$ , and
- $\text{tw}(\Gamma_{h,t}) \geq t - 1$ .

*Proof.* Complete binary trees have bounded rank-width, and Adler and Kanté prove that the linear rank-width of a forest equals its pathwidth. In particular,  $\text{lrw}(B_h) = \Omega(h)$  [AK15]. The passage from  $B_h$  to  $\Gamma_{h,t}$  is a *true-twin substitution*, i.e. replacing each vertex by a set of pairwise-adjacent vertices that share its open neighborhood; such substitutions are standard in the rank-width graph-operation view [CK09]. Here, the required bound is immediate: Take a constant-width rank-decomposition of  $B_h$  and replace each leaf  $v$  by a small subcubic tree whose leaves are the vertices of  $K_t^v$ . Across cuts inherited from  $B_h$ , the cut matrix is obtained from the cut matrix of  $B_h$  by duplicating rows and columns, so the rank does not increase. Across cuts that split a single twin clique, all rows on one side are equal, so the cut rank is at most 1. Hence  $\text{rw}(\Gamma_{h,t}) = O(1)$ .

For the linear-rank-width lower bound, choose one representative from every clique  $K_t^v$ . The induced subgraph on these representatives is  $B_h$ . Linear rank-width is monotone under vertex deletion by restricting a linear layout and deleting the corresponding rows and columns from each cut matrix. Therefore

$$\text{lrw}(\Gamma_{h,t}) \geq \text{lrw}(B_h) = \Omega(h).$$

Finally,  $\Gamma_{h,t}$  contains an induced clique  $K_t^v$ , so  $\text{tw}(\Gamma_{h,t}) \geq \text{tw}(K_t) = t - 1$ .  $\square$

**Corollary 2** (Bounded-rank-width circuits with growing competing parameters). *For every  $h$  and  $t \geq 1$  there is a circuit  $C_{h,t}$  over  $\{\text{H}, \text{CZ}\}$  such that its SOP variable graph  $G_{C_{h,t}}$  satisfies*

- $\text{rw}(G_{C_{h,t}}) = O(1)$ ,
- $\text{lrw}(G_{C_{h,t}}) = \Omega(h)$ , and
- $\text{cc}(N_{C_{h,t}}) = \Omega(t)$ .

Consequently, the rank-width DP has bounded parameter on this family, while linear rank-width grows with  $h$  and contraction complexity grows with  $t$ .

*Proof.* Apply [Lemma 3](#) to  $\Gamma_{h,t}$ , and call the resulting circuit  $C_{h,t}$ . After the input and output pins are substituted, the SOP variable graph is

$$G_{C_{h,t}} = \Gamma_{h,t}.$$

The rank-width and linear-rank-width claims follow from [Lemma 4](#).

For contraction complexity, [Lemma 1](#) gives

$$\text{tw}(G_{C_{h,t}}) \leq \text{tw}(L(N_{C_{h,t}})) = \text{cc}(N_{C_{h,t}}).$$

Since  $G_{C_{h,t}} = \Gamma_{h,t}$  contains a clique of size  $t$ , [Lemma 4](#) gives  $\text{tw}(G_{C_{h,t}}) \geq t - 1$ . Hence  $\text{cc}(N_{C_{h,t}}) = \Omega(t)$ .  $\square$

The case  $t = 1$  already separates rank-width from linear rank-width: the SOP variable graph is a complete binary tree, so the rank-width is bounded while the linear rank-width grows with the height. Increasing  $t$  makes the tensor-network contraction complexity grow as well, without changing the rank-width bound. For instance, choosing  $t = 2^h$  gives circuits of size  $\Theta(2^h t^2)$  whose rank-width parameter is constant and whose contraction complexity is  $\Omega(t)$ . This is a separation between the structural parameters used by the three algorithmic routes; it is not a lower bound against simulators using additional structure outside these parameters.

## 6 Consequences for quantum-circuit simulation

We now turn from the algorithm to what it means for simulation. We state the rank-width guarantee for circuit amplitudes ([Section 6.1](#)), show that it covers far more than  $\{\text{H}, \text{T}, \text{CZ}\}$ , and place it alongside the decision-diagram and model-counting simulators ([Section 6.3](#)).

### 6.1 Rank-width FPT simulation

Applying the rank-decomposition dynamic program of [Section 4](#) to the SOP variable graph  $G_C$  of a circuit  $C$  over  $\{\text{H}, \text{T}, \text{CZ}\}$  evaluates the amplitude  $\langle \mathbf{z} | C | \mathbf{y} \rangle$ . By [[WCYJ25](#), [CWD<sup>+</sup>25](#)] the amplitude equals the SOP value  $Z$  on  $G_C$ , so [Theorem 3](#) computes it in time  $O(|C| r 4^k \text{poly}(|C|) + r \log r)$  given a rank-decomposition of  $G_C$  of width  $k$ ; for a fixed gate set and modulus this is  $2^{O(k)} \text{poly}(|C|)$ , fixed-parameter tractable in the rank-width of  $G_C$ . The algorithm uses only the graph, its coefficients, and the rank-decomposition, so the same bound holds for any quadratic SOP, not only circuit amplitudes.

### 6.2 Diagonal gates and the Clifford+T gate set

The path-sum construction of [Section 3](#) uses only two features of the gate set, and both extend well beyond  $\{\text{H}, \text{T}, \text{CZ}\}$ ; consequently the results of the paper apply to a substantially larger class of circuits.

The first feature is that H is the only nondiagonal gate. As recalled in [Section 3](#), writing  $H_{p,q} = \frac{1}{\sqrt{2}}(-1)^{pq}$  shows that each H pairs the path value  $x$

before it with a fresh value  $x'$  after it, contributing the quadratic sign  $(-1)^{xx'} = \omega_r^{(r/2)xx'}$  and a scalar  $1/\sqrt{2}$ , while CZ contributes the same quadratic sign between two wires. We keep the standard normalized H: the  $1/\sqrt{2}$  factors are constants, collected once per Hadamard into the normalization  $R$ . These quadratic signs are exactly the edges of the SOP variable graph  $G_C$ .

The second feature is that T contributes only a diagonal phase. Replacing it by an arbitrary diagonal single-qubit gate

$$D_{\alpha,\beta} = \begin{bmatrix} \alpha & 0 \\ 0 & \beta \end{bmatrix}$$

changes nothing structurally: being diagonal,  $D_{\alpha,\beta}$  leaves the value on its wire unchanged and contributes the unary factor  $\alpha$  at  $x = 0$  and  $\beta$  at  $x = 1$ . It thus couples no wires and adds no edge to  $G_C$ , only a unary weight. Folding the scalar  $\alpha$  into  $R$  leaves weights 1 and  $\beta/\alpha$ ; when these phases are commensurate—powers of a common root of unity  $\omega_r$ —they are exactly the unary coefficients  $\omega_r^{b_v}$  of Equation 2. Diagonal gates of this form include the phase gates S, T, and Z, global-phase gates, and Z-rotations through rational multiples of  $\pi$ .

Hence every circuit over  $\{H, D_{\alpha,\beta}, CZ\}$  produces, after pinning the input and output basis states, a quadratic SOP of the form Equation 2: the H and CZ gates give the cross-terms with coefficient  $r/2$ , the diagonal gates give the unary coefficients  $b_v$ , and any interaction whose endpoints are both pinned folds into the constant  $c$ . Since CZ and CX differ only by local Hadamards (Section 2.2), this gate set realizes  $\{H, T, CX\}$ ; and because the Clifford group is generated by H, the phase gate  $S = D_{1,i}$ , and CX [NC10], it realizes all of Clifford+T, whose phases are 8th roots of unity so that again  $r = 8$ . Every result of the paper then holds verbatim for such circuits—the rank-width dynamic program (Theorem 2, Theorem 3), the treewidth and contraction-complexity bounds of Section 3.2, and the simulation guarantee of Section 6.1—since these depend only on the quadratic SOP and its variable graph  $G_C$ , not on the specific gates that produced it.

### 6.3 Knowledge-representation simulators

The SOP is exactly the kind of object that knowledge-representation methods evaluate, and our results pin down what each costs. Decision-diagram simulators [WCYJ25, CWD<sup>+</sup>25] process the variables in a fixed linear order, so on the SOP core they are governed by linear rank-width; since  $\text{rw}(G) \leq \text{lrw}(G)$  with an unbounded gap on natural families (Corollary 2), the rank-width dynamic program of Section 4 strictly strengthens this dependence while recovering it as a special case (Corollary 1).

The SOP can equally be handed to a weighted model counter [vdELLB26, MBL24, QMCL24, HCC<sup>+</sup>26]. The standard encoding introduces one Boolean *sign variable*  $s_{uv}$  per edge  $\{u, v\} \in E$ , constrained by  $s_{uv} \leftrightarrow (x_u \wedge x_v)$  and weighted  $-1$  when true, so that summing it out reproduces the cross-term sign  $(-1)^{x_u x_v}$  of Equation 2; the amplitude is then a weighted model count of the resulting formula  $F_C$ . Each sign variable is local to one edge, so the treewidth of the formula’s incidence graph, i.e. the bipartite variable-clause graph  $I(F_C)$  whose edges represent variable inclusion in clauses, stays within a constant of that of  $G_C$ .

**Lemma 5** (Variable-to-incidence treewidth transfer). *Let  $G_C$  be the SOP variable graph and  $F_C$  the model-counting encoding above. Then  $\text{tw}(I(F_C)) \leq \max(\text{tw}(G_C), 3)$ .*

*Proof.* Take a tree decomposition of  $G_C$ . For each edge  $e = \{x, y\}$  choose a bag containing both endpoints and attach a fresh leaf bag holding  $x, y, s_e$ , together with constant-size bags for the three clauses defining  $s_e$ . Every sign variable and clause vertex occurs only in this local subtree, all incidence edges are covered, and the largest new bag has size at most 4.  $\square$

Combined with  $\text{tw}(G_C) \leq \text{cc}(N_C)$  (Lemma 1), a standard model-counting dynamic program [BDP03, SS10] therefore simulates  $C$  in time  $2^{O(\text{cc}(N_C))} \text{poly}(|C|)$ , matching Markov–Shi. Rank-width, by contrast, must be measured on  $G_C$  and not on  $F_C$ . This is because the sign variables are harmless for treewidth but not for rank-width. Concretely,  $K_n$  has rank-width 1, while the incidence graph of its encoding forces rank-width linear in  $n$ . Model counting can thus be seen as a route that *exposes* the SOP, but the rank-width algorithm must run on the variable graph itself.

**Take-home message for practical matters:** General-purpose decision-diagram and model-counting engines can serve as the simulation workhorse, and the SOP structure lets one dispatch a specialized fixed-parameter algorithm (i.e. the new rank-width dynamic program of Section 4, or treewidth bucket elimination) whenever the corresponding width of  $G_C$  is small. Established weighted model counters, like Ganak [SRSM19], do implement heuristics based on treewidth decompositions. Developing improved heuristics based on treewidth and rank-width decompositions for simulation via model counting is an interesting direction for future work.

## References

- [AK15] Isolde Adler and Mamadou Moustapha Kanté. [Linear rank-width and linear clique-width of trees](#). *Theoretical Computer Science*, 589:87–98, 2015.
- [BDP03] Fahiem Bacchus, Shannon Dalmao, and Toniann Pitassi. [Algorithms and complexity results for #SAT and Bayesian inference](#). In *Proceedings of the 44th Annual IEEE Symposium on Foundations of Computer Science*, pages 340–351. IEEE Computer Society, 2003.
- [Bod96] Hans L. Bodlaender. [A linear-time algorithm for finding tree-decompositions of small treewidth](#). *SIAM J. Comput.*, 25(6):1305–1317, 1996.
- [CK09] Bruno Courcelle and Mamadou Moustapha Kanté. [Graph operations characterizing rank-width](#). *Discrete Applied Mathematics*, 157(4):627–640, 2009.
- [CL26] Julien Codsı and Tuomas Laakkonen. [Unifying graph measures and stabilizer decompositions for the classical simulation of quantum circuits](#), 2026.

- [CT65] James W. Cooley and John W. Tukey. [An algorithm for the machine calculation of complex Fourier series](#). *Mathematics of Computation*, 19(90):297–301, 1965.
- [CWD<sup>+</sup>25] Bin Cheng, Ziyuan Wang, Ruixuan Deng, Jianxin Chen, and Zhengfeng Ji. [Breaking the treewidth barrier in quantum circuit simulation with decision diagrams](#). *CoRR*, abs/2510.06775, 2025.
- [Dec99] Rina Dechter. [Bucket elimination: A unifying framework for reasoning](#). *Artificial Intelligence*, 113(1-2):41–85, 1999.
- [DHM<sup>+</sup>05] Christopher M. Dawson, Andrew P. Hines, Duncan Mortimer, Henry L. Haselgrove, Michael A. Nielsen, and Tobias J. Osborne. [Quantum computing and polynomial equations over the finite field  \$\mathbb{Z}\_2\$](#) . *Quantum Info. Comput.*, 5(2):102–112, 2005.
- [GKSS22] Robert Ganian, Eun Jung Kim, Friedrich Slivovsky, and Stefan Szeider. [Sum-of-products with default values: Algorithms and complexity results](#). *J. Artif. Intell. Res.*, 73:535–552, 2022.
- [HCC<sup>+</sup>26] Wei-Jia Huang, Christophe Charetton, Yu-Fang Chen, Kai-Min Chung, Min-Hsiu Hsieh, Alfons Laarman, and Jingyi Mei. [Equivalence checking of quantum circuits via path-sum and weighted model counting](#), 2026.
- [HiO08] Petr Hliněný and Sang il Oum. [Finding branch-decompositions and rank-decompositions](#). *SIAM Journal on Computing*, 38(3):1012–1032, 2008.
- [iO17] Sang il Oum. [Rank-width: Algorithmic and structural results](#). *Discrete Applied Mathematics*, 231:15–24, 2017.
- [iOS06] Sang il Oum and Paul Seymour. [Approximating clique-width and branch-width](#). *Journal of Combinatorial Theory, Series B*, 96(4):514–528, 2006.
- [KK26] Fedor Kuyanov and Aleks Kissinger. [Efficient classical simulation of low-rank-width quantum circuits using ZX-calculus](#), 2026.
- [MBL24] Jingyi Mei, Marcello M. Bonsangue, and Alfons Laarman. [Simulating quantum circuits by model counting](#). In *Computer Aided Verification*, Lecture Notes in Computer Science, pages 555–578. Springer, 2024.
- [MS08] Igor L. Markov and Yaoyun Shi. [Simulating quantum computation by contracting tensor networks](#). *SIAM Journal on Computing*, 38(3):963–981, 2008.
- [NC10] Michael A. Nielsen and Isaac L. Chuang. *Quantum Computation and Quantum Information*. Cambridge University Press, 10th anniversary edition, 2010.
- [Oum08] Sang-il Oum. Rank-width is less than or equal to branch-width. *Journal of Graph Theory*, 57(3):239–244, 2008.

- [QMCL24] Arend-Jan Quist, Jingyi Mei, Tim Coopmans, and Alfons Laarman. [Advancing quantum computing with formal methods](#). In *FM (2)*, Lecture Notes in Computer Science, pages 420–446. Springer, 2024.
- [SRSM19] Shubham Sharma, Subhajit Roy, Mate Soos, and Kuldeep S. Meel. [GANAK: A scalable probabilistic exact model counter](#). In Sarit Kraus, editor, *Proceedings of the Twenty-Eighth International Joint Conference on Artificial Intelligence, IJCAI 2019, Macao, China, August 10-16, 2019*, pages 1169–1176. ijcai.org, 2019.
- [SS10] Marko Samer and Stefan Szeider. [Algorithms for propositional model counting](#). *Journal of Discrete Algorithms*, 8(1):50–64, 2010.
- [vdELLB26] Dirck van den Ende, Joon Hyung Lee, Alfons Laarman, and Henning Basold. [Quantum physics using weighted model counting](#), 2026.
- [WCYJ25] Ziyuan Wang, Bin Cheng, Longxiang Yuan, and Zhengfeng Ji. [FeynmanDD: Quantum circuit analysis with classical decision diagrams](#). In *Computer Aided Verification*, volume 15934 of *Lecture Notes in Computer Science*, pages 28–52. Springer, 2025.